

Symmetry analysis and multipole classification of eigenmodes in electromagnetic resonators for engineering their optical properties

Sergey Gladishev,¹ Kristina Frizyuk,¹ and Andrey Bogdanov¹

¹*ITMO University, St. Petersburg 197101, Russia*

(Dated: January 2019)

The resonator is one of the main building blocks of a plethora of photonic and microwave devices from nanolasers to compact biosensors and magnetic resonance scanners. The symmetry of the resonators is tightly related to their mode structure and multipole content which determines the linear and non-linear response of the resonator. Here, we develop the algorithm for the classification of eigenmodes in resonators of the simplest shapes depending on their symmetry group. For each type of mode, we find its multipole content. As an illustrative example, we apply the developed formalism to the analysis of dielectric triangular prism and demonstrate the formation of high-Q resonances originated due to suppression of the scattering through the main multipole channel. The developed approach one to engineer, predict, and explain scattering phenomena and optical properties of resonators and meta-atoms basing only on their symmetry without the need for numerical simulations, and it can be used for the design of new photonic and microwave devices.

I. INTRODUCTION

Dielectric particles with high refractive index recently recommended themselves as a very prospective tool for light manipulation at the nanoscale. Their unique optical properties appear owing to Mie resonances, which can be excited even in the visible or near-infrared ranges for nanoscale particles [1–3]. Today dielectric particles with high refractive index have shown their for second [4–7] and third [8–10] harmonic generation, sensing [11], efficiency light localization [12], enhancement of the outcoupling radiation [13, 14], excitation of guided modes [15–18], heating [19], enhancement of Raman scattering [20] etc. Along with low absorption in the visible and infrared ranges, an essential advantage of dielectric particles on their plasmonic counterpart is a pronounced magnetic response. Interplay between Mie resonances results in many beautiful phenomena like directional light scattering [21–26], anapole and invisibility [27–31], supercavity mode [32, 33], electromagnetically-induced-transparency [34] etc. All these effects can be easily explained in terms of multipole expansion formalism [35–37]. The multipole formalism is very natural and convenient for small particles, when only several first resonances are essential. Thus, the Kerker effect is explained by constructive interference of electric and magnetic dipole resonances [38], supercavity mode can be explained as cancelation of the dominant multipole moment of the mode. The selection rules for nonlinear harmonic generation in nanoantennas can be easily formulated in terms of multipole moments [39, 40]. Multipole formalism allows us to better study the properties of the eigenmodes of plasmon nanoparticles [41, 42].

However, a one-to-one correspondence between the modes and multipoles can be set only for spherical resonators (spheres, core-shell particles, voids, etc). It occurs because of the angular part of the modes can be separated from the radial part of the wavefunction only for objects with spherical symmetry. Pure spherical res-

onators in a homogeneous environment are found in colloidal solutions or atmospheric physics but for integrated photonics, this is a rather unique case due to the inability to fabricate a spherical resonator by lithographic methods. For non-spherical resonators, even for a sphere on a substrate, the eigenmodes are contributed by an infinite series of the multipole moments, which depends on the symmetry of the resonator. The knowledge of the specific multipole composition of the eigenmodes depending on the resonator's symmetry is very important for engineering photonics structures with on-demand optical properties.

In this work, we provide a comprehensive multipole analysis for non-spherical resonators. Using the group-theoretical approach, we classify the mode types in resonators of different shapes and find the specific multipole series inherit to each type of the modes. In particular, we consider the resonators of the symmetry group of the cylinder, cone, cube, triangular and quadratic prisms, and chiral resonator. As an illustrative example, we apply the developed formalism to the dielectric triangular prism and analyze the evolution of the multipole content of the modes with the geometrical aspect ratio of the prism. We found a supercavity mode for the specific aspect ratio, when the radiative losses through the dominant multipole channel disappear and the quality factor demonstrates giant growth.

II. ANALYSIS OF MULTIPOLE CONTENT

The eigenmodes of a homogeneous dielectric sphere $\mathcal{E}_s(\mathbf{r})$ known as quasi-normal modes [43] or resonant states [44] are contributed by the single multipole moments. In other terms, each resonant state contains only one vector spherical harmonic (VSH) and $\mathcal{E}_s(\mathbf{r}) \sim \mathbf{W}_s(\mathbf{r})$. Here, index s is a set of the indices $\{t, p, m, l\}$ encoding the VSH \mathbf{W}_{tpml} . Index $l = 0, 1, 2, \dots$ is the total angular momentum quantum number, and $m = 0, 1, \dots, l$

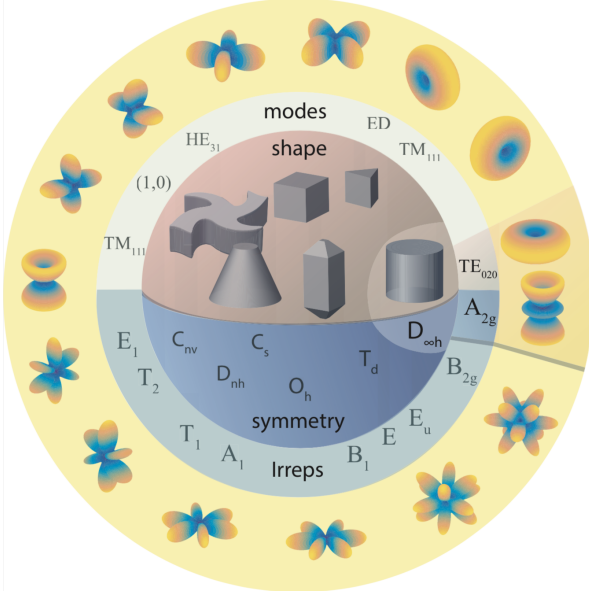


Figure 1. Sketch showing the main idea of the paper. The resonators of different shapes can be classified according to their group symmetry and their eigenmodes are classified according to the irreducible representations of the resonator's symmetry group. Each irreducible representation can be characterized by a set of vector spherical harmonics defining the multipole content of each mode.

is the absolute value of the projection of the angular momentum (magnetic quantum number). Index $p = \pm 1$ defines the parity of \mathbf{W}_s with respect to reflection from the xz -plane ($\varphi \rightarrow -\varphi$). If $p = \pm 1$ then $\mathbf{W}_s \rightarrow \pm \mathbf{W}_s$ under reflection from the xz -plane. Let us note that this definition of parity differs from that given in Ref. [1]. Index t denotes the polarization of the VSH and parity under inversion transformation. We put $t = (-1)^{l+1}$ for the magnetic VSHs (usually denoted as \mathbf{M}) and we put $t = (-1)^l$ for the electric VSHs (usually denoted as \mathbf{N}) (see, e.g., Ref. [1]). More detailed information about VSHs is provided in Appendix A. All these states form a complete set and, therefore, any eigenstate of a non-spherical resonator \mathbf{E}_q can be expanded into the series of $\mathcal{E}_s(\mathbf{r})$ [45]:

$$\mathbf{E}_q(\mathbf{r}) = \sum_s C_s^q \mathcal{E}_s(\mathbf{r}). \quad (1)$$

Therefore, the multipole content of $\mathbf{E}_q(\mathbf{r})$ is completely determined by the set of resonant states $\mathcal{E}_s(\mathbf{r})$ contributing to this mode. Strictly speaking expansion (1) also contains longitudinal (non-solenoidal) harmonics \mathbf{L} [46]. This fact does not affect the further symmetry analysis because the harmonics \mathbf{N} and \mathbf{L} with the same indices have the same symmetry with the respect to the transformations of $O(3)$ group [46]. Some coefficients in Eq. (1) can vanish in virtue of the symmetry of the mode $\mathbf{E}_q(\mathbf{r})$, which in turn is determined by the symmetry of the resonator. There are two ways to find non-vanishing coefficients.

The first way is to use the fact that eigenmodes are transformed according to irreducible representations of the symmetry group of the resonator [47]. Thus, we have the one-to-one correspondence between the irreducible representations and the types of the eigenmodes of the resonator, and each eigenmode corresponding to a certain irreducible representation consists of only those VSHs, which are transformed according to the same irreducible representation. The irreducible representations are well known for all point symmetry groups in three-dimensional space [48]. To find the VSHs composing the basis of a certain irreducible representation it is possible to use the projection operator [49, 50] which helps to bring the transformation matrices to a block diagonal form. The transformation matrices are obtained by substituting the particular angles into D-Wigner matrices (Appendix B). To avoid dealing with D-Wigner matrices we can use the fact that electric VSHs are transformed as scalars harmonics under rotations and inversion in $O(3)$ and magnetic VSHs are transformed in an opposite way under inversion, i.e. as pseudo-tensors. For some particular groups, the symmetry behavior of VSHs is analyzed in literature (see, e.g., [40, 50]).

The second way to find non-vanishing coefficients in Eq. (1) is based on the resonant state expansion scheme [44]. This way doesn't require the irreducible representation formalism to find the multipolar content of each mode. Let us focus on this way more detailed.

Any finite dielectric resonator can be represented as a perturbation of the circumscribed sphere (see Fig. 2). The resonant state of a non-spherical resonator $\mathbf{E}_q(\mathbf{r})$ satisfy the Helmholtz equation with open boundary condition (Sommerfeld boundary condition):

$$\nabla \times \nabla \times \mathbf{E}_q = [\varepsilon(\mathbf{r}) - \Delta \varepsilon(\mathbf{r})] \frac{\Omega_q^2}{c^2} \mathbf{E}_q. \quad (2)$$

It follows from the generalized Brillouin-Wigner perturbation theory [51] that coefficients C_s^q satisfy the following linear system:

$$\frac{1}{\omega_s} \sum_{s'} [\delta_{ss'} + V_{ss'}] C_{s'}^q = \frac{1}{\Omega_q} C_s^q. \quad (3)$$

Here ω_s and Ω_q are the complex eigenfrequency corresponding to $\mathcal{E}_s(\mathbf{r})$ and $\mathbf{E}_q(\mathbf{r})$, respectively. The matrix elements $V_{ss'}$ defined as

$$V_{ss'} = -\frac{1}{2} \int \Delta \varepsilon(\mathbf{r}) \mathcal{E}_s(\mathbf{r}) \cdot \mathcal{E}_{s'}(\mathbf{r}) d\mathbf{r} \quad (4)$$

$$V_{ss'} \sim \int \Delta \varepsilon(\mathbf{r}) \mathbf{W}_s(\mathbf{r}) \cdot \mathbf{W}_{s'}(\mathbf{r}) d\mathbf{r} \quad (5)$$

are responsible for the coupling between different resonant states with indices s and s' in the perturbed resonator.

According to the selection rule theorem for matrix elements [52], such an integral over the nanoparticle's volume is nonzero only if the integrand is invariant with

respect to all transformations of the particle's symmetry group. That is why we are interested only in symmetry behavior of the vector spherical harmonics. Harmonics \mathbf{W}_{tpml} and $\mathbf{W}_{t'p'm'l'}$ belong to the similar mode, if the integral in Eq. (5) is non-zero. The product of VSHs can be expanded into a series of scalar tesseral spherical harmonics ψ_{pml} as follows [39]:

$$\mathbf{W}_{tpml} \cdot \mathbf{W}_{t'p'm'l'} = \sum_{\substack{m''=|m \pm m'| \\ |l-l'| \leq l'' \leq l+l'}} \mathbb{1}_{tt'}^{l''} a_{p''m''l''}(r) \psi_{p''m''l''}. \quad (6)$$

Here ψ_{pml} are the functions invariant with respect to symmetry transformations of the resonator, index $p'' = pp'$, and $a_{p''m''l''}(r)$ is the function of radius-vector r . Indicator $\mathbb{1}_{tt'}^{l''}$ shows that the sum is taken over even l'' if $tt' = 1$ and the sum is taken over odd l'' if $tt' = -1$.

In order to find all \mathbf{W}_{tpml} contributing to a certain mode one can follow the following algorithm:

1. Find the functions $\psi_{p''m''l''}$, which are invariant with respect to symmetry transformations of the resonator. The simplest way to this is just have a look at images of the scalar spherical harmonics (see Fig. 8) and an image of $\Delta\epsilon$.
2. Take an arbitrary function \mathbf{W}_{tpml} . It is convenient to consider the function with the lowest indices. For instance, a function corresponding to magnetic or electric dipole.
3. Find harmonics $\mathbf{W}_{t'p'm'l'}$ coupled to \mathbf{W}_{tpml} using the following relations:

- (a) $t' = (-1)^{l''} t$;
- (b) $p' = p''/p$;
- (c) search all l' such as $|l - l'| \leq l'' \leq l + l'$;
- (d) search all m' such as $m' \leq l'$ and $m'' = |m \pm m'|$;

Repeating this procedure for different initial functions \mathbf{W}_{tpml} and $\psi_{p''m''l''}$ we will find that all VSHs are divided into groups. Each of these groups corresponds to some irreducible representation. Therefore, the proposed algorithm gives a way to classify the modes of resonators and find the multipole series contributing to each mode type.

III. RESULTS OF MULTIPOLE ANALYSIS

A. Cylindrical resonators

As an illustrative example, we consider a resonator with $D_{\infty h}$ symmetry. It can be a micro-pillar, dimer, or a simple cylindrical resonator in a homogeneous environment [see Fig. 2(a)]. For instance, we will consider

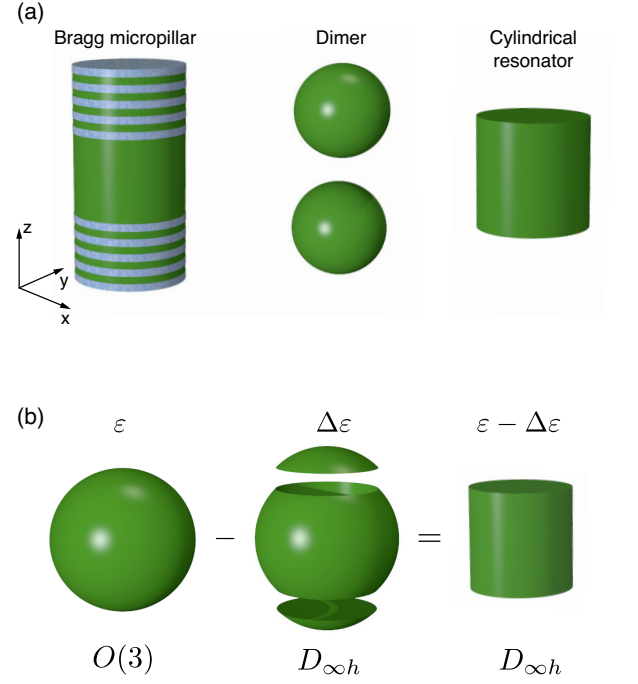


Figure 2. (a) Examples of different resonators of the same symmetry group $D_{\infty h}$. (b) Transformation the sphere [$O(3)$ group] with dielectric susceptibility ϵ to the resonator ($D_{\infty h}$ group) with dielectric susceptibility $\epsilon + \Delta\epsilon$.

a cylindrical resonator. In virtue of the axial symmetry, this group has infinite number of irreducible representations corresponding to different magnetic quantum numbers m . Table 3 shows the result, namely, the classification of the modes in resonators with $D_{\infty h}$ symmetry and the multipole content of each type of the modes. Let us show, how this table can be constructed using the proposed algorithm.

1. In virtue of the symmetry of $\Delta\epsilon$ for the cylindrical resonator, the invariant functions $\psi_{p''m''l''}$ should be even under inversion and invariant with respect to the rotation by an arbitrary angle around the z -axis. Therefore, $p'' = 1$, $m'' = 0$, and $l'' = 2k$, where k is a positive integer.
2. Now let us consider, for example, harmonic $\mathbf{W}_{-1101} = \mathbf{N}_{101}$ corresponding to the electric dipole oriented along the z -axis. Therefore, $t = -1$, $p = 1$, $m = 0$, and $l = 1$.
3. According to the proposed algorithm, this harmonics can be coupled only to the harmonics with $t' = -1$, $p' = 1$, and $m' = 0$. It follows from inequality $|1 - l'| \leq 2k \leq 1 + l'$ that l' is an arbitrary positive integer. However, all the harmonics $\mathbf{W}_{-110l'} = \mathbf{0}$, when l' is even. Therefore, all electrical harmonics $\mathbf{N}_{10(2k-1)}$ are coupled in the resonators of $D_{\infty h}$ symmetry and they do not couple to any other harmonics.



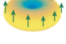



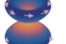

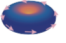



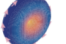
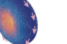

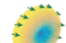


















Azimutal number	 $D_{\infty v}$ Irrep, dim	 $D_{\infty h}$ Irrep, dim	Parity	Spherical Multipoles	
				Electric	Magnetic
$m = 0$	$A_1, (1)$	$A_{1u}, (1)$	odd	N_{101}  N_{103}  $N_{10(2k-1)}$	—
		$A_{1g}, (1)$	even	N_{102}  N_{104}  $N_{10(2k)}$	—
	$A_2, (1)$	$A_{2u}, (1)$	odd	—	M_{-102}  M_{-104}  $M_{-10(2k)}$
		$A_{2g}, (1)$	even	—	M_{-101}  M_{-103}  $M_{-10(2k-1)}$
$m = 1$	$E_1, (2)$	$E_{1g}, (2)$	odd	$N_{\pm 112}$   $N_{\pm 11(2k)}$	$M_{\pm 111}$   $M_{\pm 11(2k-1)}$
		$E_{1u}, (2)$	even	$N_{\pm 111}$   $N_{\pm 11(2k-1)}$	$M_{\pm 112}$   $M_{\pm 11(2k)}$
$m = 2$	$E_2, (2)$	$E_{2u}, (2)$	odd	$N_{\pm 123}$   $N_{\pm 12(2k-1)}$	$M_{\pm 122}$   $M_{\pm 12(2k)}$
		$E_{2g}, (2)$	even	$N_{\pm 122}$   $N_{\pm 12(2k)}$	$M_{\pm 123}$   $M_{\pm 12(2k-1)}$
$m = 3$	$E_3, (2)$	$E_{3g}, (2)$	odd	$N_{\pm 134}$   $N_{\pm 13(2k)}$	$M_{\pm 133}$   $M_{\pm 13(2k-1)}$
		$E_{3u}, (2)$	even	$N_{\pm 133}$   $N_{\pm 13(2k-1)}$	$M_{\pm 134}$   $M_{\pm 13(2k)}$

Figure 3. The classification of modes by representations and the multipole composition of eigenmode for cone ($D_{\infty v}$ group), cylinder ($D_{\infty h}$ group). For each mode type showed the dimension of irreducible representations and found specific series of VSHs N_{pml} and M_{pml} . Index l expressed in k , which is a positive integer.

All harmonics $N_{10(2k-1)}$ form a basis of irreducible representation A_{1u} of $D_{\infty h}$ symmetry group (see table 3) [53–55]. Therefore, if one of these harmonics contributes to a mode, then all the rest also contribute to it. Thus, there is no need to iterate over these functions again during further analysis.

Let us repeat the procedure taking function $\mathbf{W}_{1-101} = \mathbf{M}_{-101}$ for the first step. Thus, $t = 1$, $p = -1$, $m = 0$, and $l = 1$. This multipole corresponds to the magnetic dipole oriented along the z -axis of the cylinder and it is often associated with the fundamental modes of the resonators made of high-refractive-index materials [12]. Following the algorithm, we can find that $t' = 1$, $p' = -1$, and $m' = 0$. Again, it follows from inequality $|1 - l'| \leq 2k \leq 1 + l'$ that l' is an arbitrary positive integer. However, all the harmonics $\mathbf{W}_{1-10l'} = \mathbf{0}$, when l' is even. Therefore, all magnetic harmonics $\mathbf{M}_{10(2k-1)}$ are coupled. They form a basis of irreducible representation A_{2g} of $D_{\infty h}$ symmetry group (see table 3).

Repeating the procedure for other harmonics with

$m = 0$, it is possible to show that magnetic harmonics $\mathbf{M}_{-10(2k)}$ are coupled and they form a basis of irreducible representation A_{2u} . The electric harmonics $N_{10(2k)}$ are also coupled and they form a basis of irreducible representation A_{1g} . Therefore, one can see that all the modes with $m = 0$ in resonators of $D_{\infty h}$ symmetry group are divided into four independent groups contributing by different multipoles. This division has the simple origin. It is well-known that for $m = 0$, the solutions of Maxwell's equations can be divided into different polarizations usually denoted as TE and TM [56]. In addition, the modes of each polarization can be divided into the odd and even with respect to reflection in the xy -plane:

$$\begin{bmatrix} E_\rho(\rho, \varphi, -z) \\ E_\varphi(\rho, \varphi, -z) \\ E_z(\rho, \varphi, -z) \end{bmatrix} = \sigma_z \begin{bmatrix} E_\rho(\rho, \varphi, z) \\ E_\varphi(\rho, \varphi, z) \\ -E_z(\rho, \varphi, z) \end{bmatrix} \quad (7)$$

If $\sigma_z = 1$ then the mode is defined as even, and if $\sigma_z = -1$ then the mode is defined as odd.

It follows from the proposed algorithm that only the

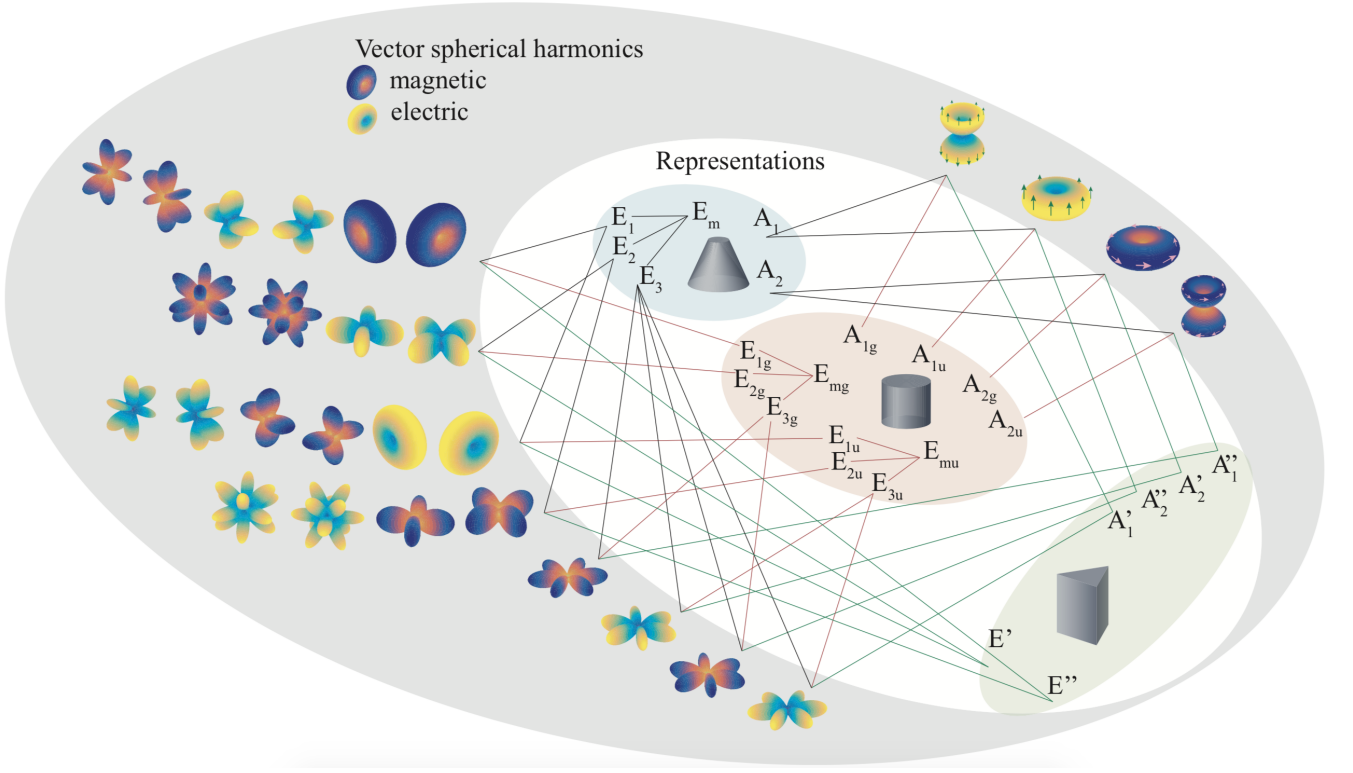


Figure 4. The classification of modes by representations and the multipole composition of each mode for cone ($D_{\infty v}$ group), cylinder ($D_{\infty h}$ group) and triangular prism (D_{3h} group).

modes with the same azimuthal index m and similar parities t and p are coupled. However, we can note that the modes with $m \neq 0$ are transformed through each other under rotations around the z -axis. Indeed, for example, the x -oriented electric dipole (\mathbf{N}_{111}) turns into the y -oriented dipole \mathbf{N}_{-111} under rotation by $\pi/2$ with respect to the z -axis. This means that these modes form a basis of high-dimensional irreducible representation and have the same energy. So, if under all possible transformations of the structure's symmetry the mode is only multiplied by some number (for example, $\mathbf{N}_{101} \rightarrow \mathbf{N}_{101}$ under rotations of the cylinder and $\mathbf{N}_{101} \rightarrow -\mathbf{N}_{101}$ under inversion), then the dimension of representation is one and the mode is not degenerate. If the mode transformed into some linear combination of itself and some other modes, then these modes are degenerate and the dimension of representation is more than one.

B. Effect of substrate

The classification of the modes in resonators of a cone symmetry ($D_{\infty v}$) can be straightforwardly obtained from the results for $D_{\infty h}$ symmetry group accounting for the fact that in $D_{\infty v}$ there is no mirror symmetry with respect to the xy -plane, and therefore, the modes are not divided into odd and even with respect to reflection in the xy -plane. Thus, for example, the basis of irreducible

representation A_1 of $D_{\infty v}$ consists of all multipoles from A_{1u} and A_{1g} of $D_{\infty h}$, as result, the even and odd mode are mixed (see table 3).

C. Other symmetry groups

Following the proposed algorithm we classify the modes and analyzed their multipole content for the groups of the triangular prism (D_{3h}), quadratic prisms (D_{4h}), cube (O_h) and chiral resonators of C_{4h} symmetry. The results of classification are shown in tables I, II, III, and in table 5. Note that for O_h and C_{4h} groups we obtain that some similar vector spherical harmonics contribute to two different irreducible representations. This happens due to the fact that only one particular linear combination contributes to one mode and different combinations into others. For the case of the O_h group, the combinations are provided in [57]. For the case of such resonators on a substrate, the even and odd modes should be mixed. Alternatively to the table form the classification could be represented graphically (see Fig. 4).

D. Bianisotropy

We can observe the destruction of bianisotropy for some modes in the transition from cone ($D_{\infty v}$ group)

Table I. The classification of modes by representations and the multipole composition of eigenmode for triangular prism (D_{3h}). For each mode type showed the dimension of irreducible representations and found specific series of VSHs \mathbf{N}_{pml} and \mathbf{M}_{pml} . Indices m and l expressed in s and k , which are positive integer, respectively.

Parity	Irrep D_{3h} , dim	Spherical Multipoles	
		Electric	Magnetic
odd	$A_1'', (1)$	$\mathbf{N}_{-1,3s,2k}$	$\mathbf{M}_{1,0,2k}, \mathbf{M}_{-1,3s,2k-1}$
	$A_2'', (1)$	$\mathbf{N}_{1,0,2k-1}, \mathbf{N}_{1,3s,2k}$	$\mathbf{M}_{1,3s,2k-1}$
	$E'', (2)$	$\mathbf{N}_{\pm 1,3s-1,2k-1}$	$\mathbf{M}_{\pm 1,3s-1,2k}$
		$\mathbf{N}_{\pm 1,3s-2,2k}$	$\mathbf{M}_{\pm 1,3s-2,2k-1}$
even	$A_1', (1)$	$\mathbf{N}_{1,0,2k}, \mathbf{N}_{1,3s,2k-1}$	$\mathbf{M}_{1,3s,2k}$
	$A_2', (1)$	$\mathbf{N}_{-1,3s,2k-1}$	$\mathbf{M}_{1,0,2k-1}, \mathbf{M}_{-1,3s,2k}$
	$E', (2)$	$\mathbf{N}_{\pm 1,3s-2,2k-1}$	$\mathbf{M}_{\pm 1,3s-2,2k}$
		$\mathbf{N}_{\pm 1,3s-1,2k}$	$\mathbf{M}_{\pm 1,3s-1,2k-1}$

Table II. The classification of modes by representations and the multipole composition of eigenmode for quadrangular prism (D_{4h}). For each mode type showed the dimension of irreducible representations and found specific series of VSHs \mathbf{N}_{pml} and \mathbf{M}_{pml} . Indices m and l expressed in s and k , which are positive integer, respectively.

Parity	Irrep D_{4h} , dim	Spherical Multipoles	
		Electric	Magnetic
odd	$A_{1u}, (1)$	$\mathbf{N}_{-1,4s,2k-1}$	$\mathbf{M}_{1,0,2k}, \mathbf{M}_{-1,4s,2k}$
	$A_{2u}, (1)$	$\mathbf{N}_{1,0,2k-1}, \mathbf{N}_{1,4s,2k-1}$	$\mathbf{M}_{1,4s,2k}$
	$B_{1u}, (1)$	$\mathbf{N}_{-1,4s-2,2k-1}$	$\mathbf{M}_{-1,4s-2,2k}$
	$B_{2u}, (1)$	$\mathbf{N}_{1,4s-2,2k-1}$	$\mathbf{M}_{1,4s-2,2k}$
	$E_g, (2)$	$\mathbf{N}_{-1,4s-3,2k}$	$\mathbf{M}_{-1,4s-3,2k-1}$
		$\mathbf{N}_{1,4s-3,2k}$	$\mathbf{M}_{1,4s-3,2k-1}$
even	$A_{1g}, (1)$	$\mathbf{N}_{1,0,2k}, \mathbf{N}_{1,4s,2k}$	$\mathbf{M}_{1,4s,2k-1}$
	$A_{2g}, (1)$	$\mathbf{N}_{-1,4s,2k}$	$\mathbf{M}_{1,0,2k-1}, \mathbf{M}_{-1,4s,2k-1}$
	$B_{1g}, (1)$	$\mathbf{N}_{1,4s-2,2k}$	$\mathbf{M}_{1,4s-2,2k-1}$
	$B_{2g}, (1)$	$\mathbf{N}_{-1,4s-2,2k}$	$\mathbf{M}_{-1,4s-2,2k-1}$
	$E_u, (2)$	$\mathbf{N}_{-1,4s-3,2k-1}$	$\mathbf{M}_{-1,4s-3,2k}$
		$\mathbf{N}_{1,4s-3,2k-1}$	$\mathbf{M}_{1,4s-3,2k}$

to cylinder ($D_{\infty h}$ group), increasing the symmetry of the particle. Bianisotropy in a single particle is shown in the form of the presence of an electric and magnetic multipole of the same order simultaneously in the eigenmode [58]. Indeed, the presence of magnetic and electric multipoles in one mode means, for example, that we can induce magnetic response by the incident wave with the symmetry of the electric dipole. The inversion symmetry forbids this effect. When structure has inversion symmetry, we can not obtain multipoles of different parity under inversion in one mode. Moreover, this is related not only to electric and magnetic multipoles of the same order, but also to any two multipoles of opposite parity.

IV. BOUND STATE IN THE CONTINUUM IN THE TRIANGULAR PRISM.

We have shown that some coefficients C_s^q in expansion (1) can be zero due to the symmetry and, thus, some VSHs are not contribute to the modes. But some of the

coefficients allowed by the symmetry analysis may vanish or be strongly suppressed accidentally for specific parameters of the resonators. In particular, change of the resonator's geometry preserving its symmetry can result in suppression of the radiative losses through multipole channels allowed by the symmetry. It results in a drastic increase of the quality factor (Q factor) and appearance of so-called *supercavity mode* or *quasi-bound state in the continuum* (quasi-BIC) [32]. This effect was studied in detail theoretically and experimentally for cylindrical resonators [59–61]. Here, we show that quasi-BIC can be observed in resonators of non-cylindrical symmetry. As an example, we consider a dielectric triangular prism with a regular triangle at the base. Permittivity of the prism ϵ is taken equal to 81. The height of the prism is L and the length of the base edge is a .

Figure 6(a) shows the dependence of dimensionless frequency ka on aspect ratio a/L , where k is the wavenumber. The blue and red curves correspond to two eigenmodes of the resonator from the same irreducible representation E'' . These modes have the same multi-

Table III. The classification of modes by representations and the multipole composition of eigenmode for cube (O_h). For each mode type showed the dimension of irreducible representations and found specific series of VSHs \mathbf{N}_{pml} and \mathbf{M}_{pml} . Indices m and l expressed in s and k , which are positive integer, respectively.

Parity	Irrep O_h , dim	Spherical Multipoles	
		Electric	Magnetic
odd	$A_{1u}, (1)$	$\mathbf{N}_{1,4s-2,2k+1}$	$\mathbf{M}_{1,4s-2,2k}$
	$A_{2u}, (1)$	$\mathbf{N}_{-1,4s-2,2k+1}$	$\mathbf{M}_{-1,4s-2,2k}$
	$E_u, (2)$	$\mathbf{N}_{-1,4s-2,2k+1}$	$\mathbf{M}_{-1,4s-2,2k}$
		$\mathbf{N}_{-1,4s,2k+1}$	$\mathbf{M}_{-1,0,2k}, \mathbf{M}_{-1,4s,2k}$
	$T_{1u}, (3)$	$\mathbf{N}_{1,4s,2k-1}, \mathbf{N}_{1,0,2k-1}$	$\mathbf{M}_{1,4s,2(k+1)}$
	$T_{2u}, (3)$	$\mathbf{N}_{1,4s-2,2k+1}$	$\mathbf{M}_{1,4s-2,2k}$
	$T_{1g}, (3)$	$\mathbf{N}_{-1,4s-3,2(k+1)}, \mathbf{N}_{-1,4s-1,2(k+1)}$	$\mathbf{M}_{-1,4s-3,2k-1}, \mathbf{M}_{-1,4s-1,2k-1}$
		$\mathbf{N}_{1,4s-3,2(k+1)}, \mathbf{N}_{1,4s-1,2(k+1)}$	$\mathbf{M}_{1,4s-3,2k-1}, \mathbf{M}_{1,4s-1,2k-1}$
	$T_{2g}, (3)$	$\mathbf{N}_{-1,4s-3,2k}, \mathbf{N}_{-1,4s-1,2k}$	$\mathbf{M}_{-1,4s-3,2k+1}, \mathbf{M}_{-1,4s-1,2k+1}$
		$\mathbf{N}_{1,4s-3,2k}, \mathbf{N}_{1,4s-1,2k}$	$\mathbf{M}_{1,4s-3,2k+1}, \mathbf{M}_{1,4s-1,2k+1}$
even	$A_{1g}, (1)$	$\mathbf{N}_{-1,4s-2,2k}$	$\mathbf{M}_{-1,4s-2,2k+1}$
	$A_{2g}, (1)$	$\mathbf{N}_{1,4s-2,2k}$	$\mathbf{M}_{1,4s-2,2k+1}$
	$E_g, (2)$	$\mathbf{N}_{1,4s-2,2k}$	$\mathbf{M}_{1,4s-2,2k+1}$
		$\mathbf{N}_{1,0,2k}, \mathbf{N}_{1,4s,2k}$	$\mathbf{M}_{1,4s,2k+1}$
	$T_{1g}, (3)$	$\mathbf{N}_{-1,4s,2k}$	$\mathbf{M}_{-1,0,2k-1}, \mathbf{M}_{-1,4s,2k-1}$
	$T_{2g}, (3)$	$\mathbf{N}_{-1,4s-2,2k}$	$\mathbf{M}_{-1,4s-2,2k-1}$
	$T_{1u}, (3)$	$\mathbf{N}_{-1,4s-3,2k-1}, \mathbf{N}_{-1,4s-1,2k-1}$	$\mathbf{M}_{-1,4s-3,2(k+1)}, \mathbf{M}_{-1,4s-1,2(k+1)}$
		$\mathbf{N}_{1,4s-3,2k-1}, \mathbf{N}_{1,4s-1,2k-1}$	$\mathbf{M}_{1,4s-3,2(k+1)}, \mathbf{M}_{1,4s-1,2(k+1)}$
	$T_{2u}, (3)$	$\mathbf{N}_{-1,4s-3,2k+1}, \mathbf{N}_{-1,4s-1,2k+1}$	$\mathbf{M}_{-1,4s-3,2k}, \mathbf{M}_{-1,4s-1,2k}$
		$\mathbf{N}_{1,4s-3,2k+1}, \mathbf{N}_{1,4s-1,2k+1}$	$\mathbf{M}_{1,4s-3,2k}, \mathbf{M}_{1,4s-1,2k}$

pole content and they can interact through the continuum [62, 63]. The interaction between these modes manifests itself as a characteristic avoid crossing. As a results of the interaction, the Q factor of one mode decreases (blue curve) and for the second mode, it increases (red curve). The dependence of Q factor on the aspect ratio L/a for these modes are shown in Fig. 6(c). One can see the Q factor of one of the mode are increased by more than two orders of magnitude from $1 \cdot 10^2$ to $3.6 \cdot 10^4$ [point B in Fig. 6(b)] in the vicinity of the avoid crossing, when a/L changes from 1.15 to 1.25. This clearly demonstrates the appearance of quasi-BIC in non-cylindrical resonators. The distribution of the electric field amplitude for the high-Q mode for different values of the aspect ration is shown in Fig. 6(b). One can see that for the aspect ration $a/L = 1.25$, when the Q factor becomes maximal, the field distribution becomes more symmetric. This indirectly indicates the suppression of scattering through the main multipole channel.

To prove that, the increase in the Q factor is the result of scattering suppression through the main multipole channel, we analyse the multipole content of the radiated field as function of the aspect ratio of the prism. It follows from the symmetry analysis (see Table I) that the lowest-order multipole contributing to the considered modes is the magnetic dipole moment ($\mathbf{M}_{\pm 1,1,1}$), next non-zero multipoles for these modes are the electric ($\mathbf{N}_{\pm 1,1,2}$) and magnetic ($\mathbf{M}_{\pm 1,2,2}$) quadrupole moments,

and the electric ($\mathbf{N}_{\pm 1,2,3}$) and magnetic ($\mathbf{M}_{\pm 1,1,3}$) octupole moments. The contribution of these multipoles to the radiated power as a function of the aspect ration is shown in Fig. 6(d). The calculations were done using the COMSOL Multiphysics software package. One can see that exactly at the point B, where the Q factor reaches the maximal value, the magnetic dipole moment of the mode is suppressed and the mode behaves as electric quadrupole. It also can be seen from the far-field radiation patterns shown in Fig. 6(e).

V. CONCLUSION

In summary, we have classified eigenmodes of the resonators of the simplest shape using the group theory analysis. For each type of the modes we found its multipole content. The proposed algorithm can be used for the resonators of arbitrary shapes made of any materials and placed into any environments. By the example of cylindrical and cone resonators, we demonstrated how their eigenmodes modes can be classified and how to find the specific multipole series inherit to each type of the modes. We presented ready-made tables of mode classification and their multipole content for resonators of cylindrical symmetry (on a substrate and in homogeneous environment), triangular and quadratic prisms, cube and chiral resonators.



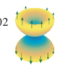
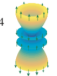
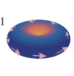
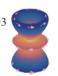
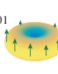
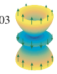
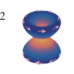
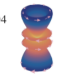

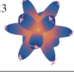
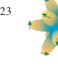
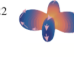

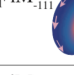



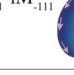
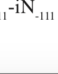
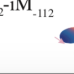
 C_{4h} Irrep, dim	 C_4 Irrep, dim	Parity	Spherical Multipoles					
			Electric			Magnetic		
A, (1)	$A_g, (1)$	even	N_{102} 	N_{104} 	$N_{1(4s)(2k)}$	M_{-101} 	M_{-103} 	$M_{-1(4s)(2k-1)}$
	$A_u, (1)$	odd	N_{101} 	N_{103} 	$N_{1(4s)(2k-1)}$	M_{-102} 	M_{-104} 	$M_{-1(4s)(2k)}$
B, (1)	$B_g, (1)$	even	$N_{\pm 122}$ 	$N_{\pm 1(4s+2)(2k)}$		$M_{\pm 123}$ 	$M_{\pm 1(4s+2)(2k-1)}$	
	$B_u, (1)$	odd	$N_{\pm 123}$ 	$N_{\pm 1(4s+2)(2k-1)}$		$M_{\pm 122}$ 	$M_{\pm 1(4s+2)(2k)}$	
E, (1)	$E_g, (1)$	even	$N_{112}^{+i}N_{-112}^{-i}$ 	$N_{\pm 1(4s\pm 1)(2k)}$		$M_{111}^{+i}M_{-111}^{-i}$ 	$M_{\pm 1(4s\pm 1)(2k-1)}$	
	$E_u, (1)$	odd	$N_{111}^{+i}N_{-111}^{-i}$ 	$N_{\pm 1(4s\pm 1)(2k-1)}$		$M_{112}^{+i}M_{-112}^{-i}$ 	$M_{\pm 1(4s\pm 1)(2k)}$	
$E^*, (1)$	$E_g^*, (1)$	even	$N_{112}^{-i}N_{-112}^{+i}$ 	$N_{\pm 1(4s\pm 1)(2k)}$		$M_{111}^{-i}M_{-111}^{+i}$ 	$M_{\pm 1(4s\pm 1)(2k-1)}$	
	$E_u^*, (1)$	odd	$N_{111}^{-i}N_{-111}^{+i}$ 	$N_{\pm 1(4s\pm 1)(2k-1)}$		$M_{112}^{-i}M_{-112}^{+i}$ 	$M_{\pm 1(4s\pm 1)(2k)}$	

Figure 5. The classification of modes by representations and the multipole composition of eigenmode for chiral resonator (C_{4h} group) and chiral resonator for slab (C_4 group). For each mode type showed the dimension of irreducible representations and found specific series of VSHs \mathbf{N}_{pml} and \mathbf{M}_{pml} . Indices m and l expressed in s and k , which are positive integer, respectively.

Many beautiful optical phenomena like anapole, invisibility, or directive light catering are usually considered only for spherical resonators because of the simplicity of their shape. However, in practice, it is difficult to have pure spherical resonators in homogeneous environment. Using the developed approach, the optical phenomena, which are explained in terms of multipole moments, can be extended beyond the resonators of spherical shape. Thus, we predicted and explained the appearance of quasi-bound state in the continuum in the triangular prism. Therefore, the developed formalism shows the beauty and power of the symmetry analysis in physics. It allows one to engineer, predict, and explain scattering phenomena and optical properties of resonators and meta-atoms basing only on their symmetry without numerical simulations, and it can be used for the design of new photonic and microwave devices.

ACKNOWLEDGMENTS

This work is supported by the Grant of the President of the Russian Federation (MK-2224.2020.2) and RFBR (19-02-00419). A.B. and K.F. acknowledge the BASIS foundation.

Appendix A: Definition of vector spherical harmonics

The vector spherical harmonics are defined in the following way:

$$\mathbf{M}_{-1mn} = \nabla \times (\mathbf{r}\psi_{-1mn}), \quad (\text{A1})$$

$$\mathbf{N}_{-1mn} = \frac{\nabla \times \mathbf{M}_{-1mn}}{k}, \quad (\text{A2})$$

$$\mathbf{L}_{-1mn} = \nabla\psi_{-1mn}, \quad (\text{A3})$$

where

$$\psi_{1mn}(kr) = z_n(kr)P_n^m(\cos\theta)\cos m\varphi, \quad (\text{A4})$$

$$\psi_{-1mn}(kr) = z_n(kr)P_n^m(\cos\theta)\sin m\varphi. \quad (\text{A5})$$

Here $z_n(kr)$ can be replaced by spherical bessel function of any kind, and $P_n^m(\cos\theta)$ is the associated Legendre polynomial.

Appendix B: Transformation of vector functions

Any point symmetry group transformation can be written as a combination of rotations and inversion, so

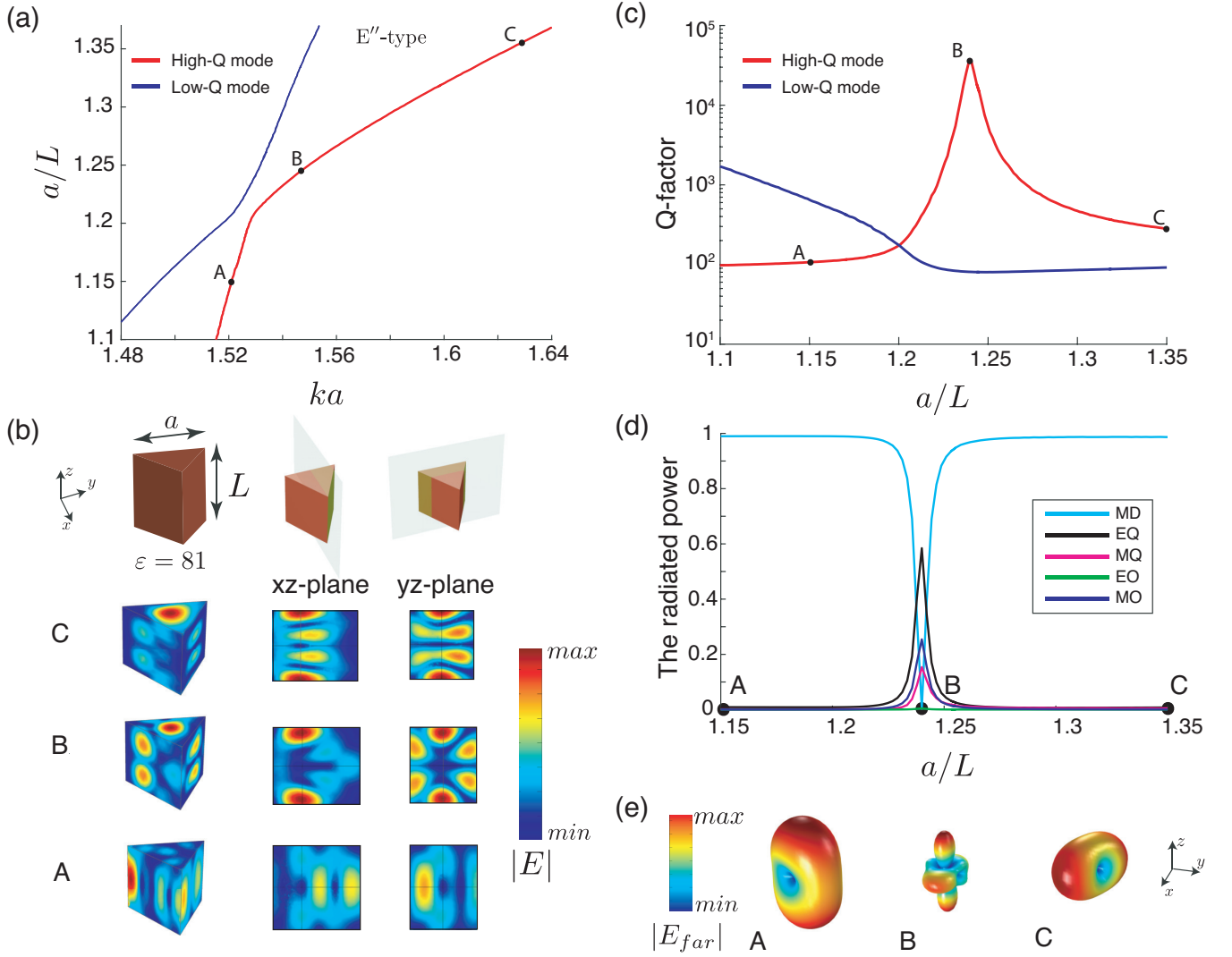


Figure 6. (a) Strong coupling of high-Q and low-Q modes of E'' -type in a dielectric triangular resonator with $\varepsilon = 81$ depending on size parameter ka and aspect ratio a/L , where k , a , and L are the wavevector in the vacuum, the side of the triangle at the base prism, and the height of the prism, respectively. (b) Distribution of the electric field amplitude $|E|$ of high-Q mode for different aspect ratios (points A, B, C). (c) Evolution of the Q-factor of two interacting modes depending on aspect ratio a/L . (d) Contribution of the electric and magnetic multipoles to the radiated power of high-Q mode. (e) Far-field radiation patterns for different aspect ratios (points A, B, C). Panel B corresponds to the supercavity mode.

there is no need to consider, for example, reflections, separately. Transformation of scalar spherical functions is given by the known formula [64]:

$$\psi_{pml}(\hat{R}^{-1}\mathbf{r}) = \sum_{m',p'} \psi_{p'm'l}(\mathbf{r}) S_{p'pm'm}^l(\hat{R}). \quad (\text{B1})$$

Here $S_{p'pm'm}^l(\hat{R})$ are the matrices which can be obtained from the law of the transformation of complex spherical functions [66]. They are specific combinations of the Wigner D-matrices [65], and \hat{R} is the rotation matrix which transforms the radius vector. Note that functions with similar l are transformed through each other and the radial part $z_n(kr)$ is not transformed under point group

transformations.

In case of inversion, the scalar spherical function are transformed as follows:

$$\psi_{pml}(-\mathbf{r}) = (-1)^l \psi_{pml}(\mathbf{r}) \quad (\text{B2})$$

One can prove that under rotations, vector spherical harmonics have similar behavior as scalar ones [67, 68], which is illustrated in Fig. 7. However, for the vector functions, the rotation can not be written in this simple way, because in order to rotate the vector function we need to rotate both the vector argument and the value of the function. It is convenient to write such a transfor-

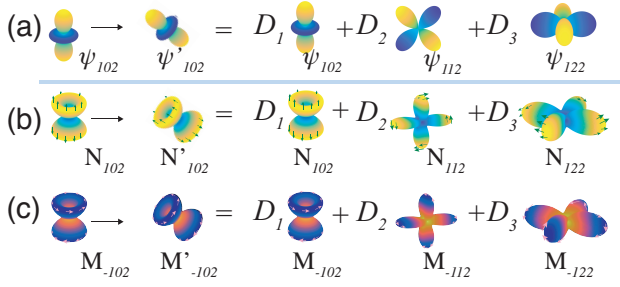


Figure 7. (a) Example of rotation transformation of the scalar spherical function ψ_{102} . The arbitrarily rotated function can be presented as linear combination of functions Y_{1m2} , and the function, rotated around the y -axis - as linear combination of functions ψ_{1m2} . (b), (c) Rotation of electric \mathbf{N}_{102} and magnetic \mathbf{M}_{-102} vector spherical harmonics is described by the similar rule, and rotated vector spherical harmonics are presented as the combination of functions \mathbf{W}_{1m2} with the same coefficients as scalar.

mation for every projection:

$$N_{x,pml}(\hat{R}^{-1}\mathbf{r})\hat{R}^{-1}\mathbf{e}_x + N_{y,pml}(\hat{R}^{-1}\mathbf{r})\hat{R}^{-1}\mathbf{e}_y + N_{z,pml}(\hat{R}^{-1}\mathbf{r})\hat{R}^{-1}\mathbf{e}_z = \sum_{m',p'} S_{p'pm'm}^l(\hat{R})\mathbf{N}_{p'm'l}(\mathbf{r}) \quad (\text{B3})$$

$$M_{x,-pml}(\hat{R}^{-1}\mathbf{r})\hat{R}^{-1}\mathbf{e}_x + M_{y,-pml}(\hat{R}^{-1}\mathbf{r})\hat{R}^{-1}\mathbf{e}_y + M_{z,-pml}(\hat{R}^{-1}\mathbf{r})\hat{R}^{-1}\mathbf{e}_z = \sum_{m',p'} S_{p'pm'm}^l(\hat{R})\mathbf{M}_{-p'm'l}(\mathbf{r}) \quad (\text{B4})$$

Matrices $S_{p'pm'm}^l(\hat{R})$ are the same as for scalar spherical functions. Note, that the rotation behavior of ψ_{pml} , \mathbf{N}_{pml} , and \mathbf{M}_{-pml} is similar.

Under inversion, the behavior of magnetic and electric harmonics is opposite. Indeed, for electric harmonics, it is similar the behavior of the scalar functions):

$$-N_{x,pml}(-\mathbf{r})\mathbf{e}_x - N_{y,pml}(-\mathbf{r})\mathbf{e}_y - N_{z,pml}(-\mathbf{r})\mathbf{e}_z = -\mathbf{N}_{pml}(-\mathbf{r}) = (-1)^l \mathbf{N}_{pml}(\mathbf{r}). \quad (\text{B5})$$

Magnetic harmonics are transformed under inversion as follows:

$$-M_{x,pml}(-\mathbf{r})\mathbf{e}_x - M_{y,pml}(-\mathbf{r})\mathbf{e}_y - M_{z,pml}(-\mathbf{r})\mathbf{e}_z = -\mathbf{M}_{pml}(-\mathbf{r}) = (-1)^{l+1} \mathbf{M}_{pml}(\mathbf{r}) \quad (\text{B6})$$

For example, the electric dipoles are odd under inversion, electric quadrupoles are even, magnetic dipoles are even, magnetic quadrupoles are odd, and so on.

-
- [1] C. F. Bohren and D. R. Huffman, *Absorption and Scattering of Light by Small Particles* (John Wiley & Sons, 2008).
 - [2] A. I. Kuznetsov, A. E. Miroschnichenko, M. L. Brongersma, Y. S. Kivshar, and B. Luk'yanchuk, Optically resonant dielectric nanostructures, *Science* **354**, aag2472 (2016).
 - [3] A. Arbabi, Y. Horie, M. Bagheri, and A. Faraon, Dielectric metasurfaces for complete control of phase and polarization with subwavelength spatial resolution and high transmission, *Nat. Nanotechnol.* **10**, 937 (2015).
 - [4] D. Smirnova, A. I. Smirnov, and Y. S. Kivshar, Multipolar second-harmonic generation by mie-resonant dielectric nanoparticles, *Phys. Rev. A* **97**, 013807 (2018).
 - [5] S. S. Kruk, R. Camacho-Morales, L. Xu, M. Rahmani, D. A. Smirnova, L. Wang, H. H. Tan, C. Jagadish, D. N. Neshev, and Y. S. Kivshar, Nonlinear optical magnetism revealed by second-harmonic generation in nanoantennas, *Nano Lett.* **17**, 3914 (2017).
 - [6] V. Gili, L. Carletti, A. Locatelli, D. Rocco, M. Finazzi, L. Ghirardini, I. Favero, C. Gomez, A. Lemaître, M. Celebrano, *et al.*, Monolithic algaas second-harmonic nanoantennas, *Opt. Express* **24**, 15965 (2016).
 - [7] S. V. Makarov, M. I. Petrov, U. Zywietz, V. Milichko, D. Zuev, N. Lopanitsyna, A. Kuksin, I. Mukhin, G. Zograf, E. Ubyivovk, *et al.*, Efficient second-harmonic generation in nanocrystalline silicon nanoparticles, *Nano Lett.* **17**, 3047 (2017).
 - [8] D. A. Smirnova, A. B. Khanikaev, L. A. Smirnov, and Y. S. Kivshar, Multipolar third-harmonic generation driven by optically induced magnetic resonances, *ACS Photonics* **3**, 1468 (2016).
 - [9] M. R. Shcherbakov, A. S. Shorokhov, D. N. Neshev, B. Hopkins, I. Staude, E. V. Melik-Gaykazyan, A. A. Ezhov, A. E. Miroschnichenko, I. Brener, A. A. Fedyanin, *et al.*, Nonlinear interference and tailorable third-harmonic generation from dielectric oligomers, *ACS Photonics* **2**, 578 (2015).
 - [10] G. Grinblat, Y. Li, M. P. Nielsen, R. F. Oulton, and S. A. Maier, Enhanced third harmonic generation in single germanium nanodisks excited at the anapole mode, *Nano Lett.* **16**, 4635 (2016).
 - [11] N. Bontempi, K. E. Chong, H. W. Orton, I. Staude, D.-Y. Choi, I. Alessandri, Y. S. Kivshar, and D. N. Neshev, Highly sensitive biosensors based on all-dielectric nanoresonators, *Nanoscale* **9**, 4972 (2017).

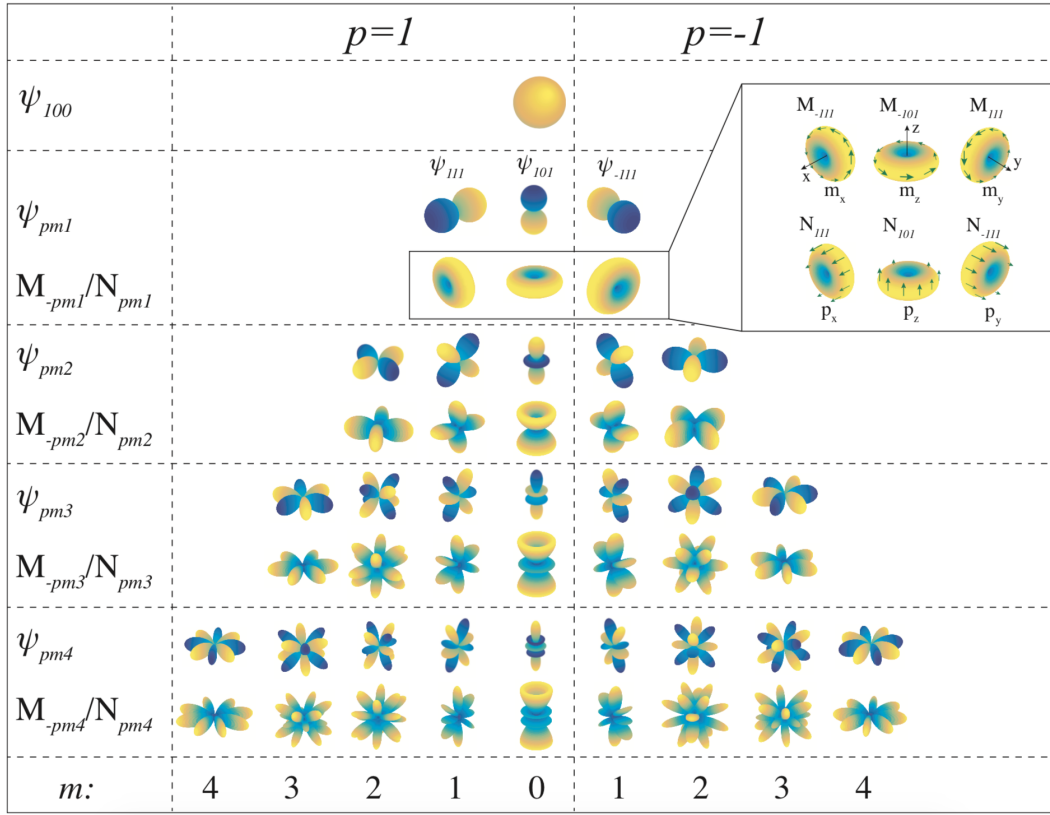


Figure 8. Scalar and vector real spherical harmonics for $n = 1, 2, 3, 4$. Only far-field radiation patterns are presented for the vector harmonics. Radiation patterns are similar for the harmonics N_{pml} and M_{-pml} , but polarization is orthogonal (example for the dipoles is in the insert).

- [12] Y. Kivshar and A. Miroshnichenko, Meta-optics with mie resonances, *Opt. Photonics News* **28**, 24 (2017).
- [13] N. Kryzhanovskaya, Y. Polubavkina, E. Moiseev, M. Maximov, V. Zhurikhina, S. Scherbak, A. Lipovskii, M. Kulagina, Y. Zadiranov, I. Mukhin, F. Komissarenko, A. Bogdanov, A. Krasnok, and A. Zhukov, Enhanced light outcoupling in microdisk lasers via Si spherical nanoantennas, *J. Appl. Phys.* **124**, 163102 (2018).
- [14] Y. S. Polubavkina, N. V. Kryzhanovskaya, E. I. Moiseev, M. M. Kulagina, I. S. Mukhin, F. E. Komissarenko, Y. M. Zadiranov, M. V. Maximov, A. E. Krasnok, A. A. Bogdanov, A. E. Zhukov, and A. V. Shelaev, Improved emission outcoupling from microdisk laser by Si nanospheres, *J. Phys. Conf. Ser.* **741**, 012158 (2016).
- [15] I. S. Sinev, A. A. Bogdanov, F. E. Komissarenko, K. S. Frizyuk, M. I. Petrov, I. S. Mukhin, S. V. Makarov, A. K. Samusev, A. V. Lavrinenko, and I. V. Iorsh, Chirality Driven by Magnetic Dipole Response for Demultiplexing of Surface Waves, *Laser Photon. Rev.* **11**, 1700168 (2017).
- [16] A. Krasnok, S. Li, S. Lepeshov, R. Savelev, D. G. Baranov, and A. Alú, All-optical switching and unidirectional plasmon launching with nonlinear dielectric nanoantennas, *Phys. Rev. Appl.* **9**, 014015 (2018).
- [17] S. V. Li, D. G. Baranov, A. E. Krasnok, and P. A. Belov, All-dielectric nanoantennas for unidirectional excitation of electromagnetic guided modes, *Appl. Phys. Lett.* **107**, 171101 (2015).
- [18] M. F. Picardi, M. Neugebauer, J. S. Eismann, G. Leuchs, P. Banzer, F. J. Rodríguez-Fortuño, and A. V. Zayats, Experimental demonstration of linear and spinning janus dipoles for polarisation- and wavelength-selective near-field coupling, *Light Sci. Appl.* **8**, 52 (2019).
- [19] G. P. Zograf, M. I. Petrov, D. A. Zuev, P. A. Dmitriev, V. A. Milichko, S. V. Makarov, and P. A. Belov, Resonant nonplasmonic nanoparticles for efficient temperature-feedback optical heating, *Nano Lett.* **17**, 2945 (2017).
- [20] K. Frizyuk, M. Hasan, A. Krasnok, A. Alú, and M. Petrov, Enhancement of raman scattering in dielectric nanostructures with electric and magnetic mie resonances, *Phys. Rev. B* **97**, 085414 (2018).
- [21] J.-M. Geffrin, B. García-Cámara, R. Gómez-Medina, P. Albella, L. Froufe-Pérez, C. Eyraud, A. Litman, R. Vaillon, F. González, M. Nieto-Vesperinas, *et al.*, Magnetic and electric coherence in forward- and back-scattered electromagnetic waves by a single dielectric subwavelength sphere, *Nat. Commun.* **3**, 1171 (2012).
- [22] H. K. Shamkhi, K. V. Baryshnikova, A. Sayanskiy, P. Kapitanova, P. D. Terekhov, P. Belov, A. Karabchevsky, A. B. Evlyukhin, Y. Kivshar, and A. S. Shalin, Transverse scattering and generalized kerker effects in all-dielectric mie-resonant metaoptics, *Phys. Rev. Lett.* **122**, 193905 (2019).
- [23] P. Jin and R. W. Ziolkowski, Metamaterial-inspired, electrically small huygens sources, *IEEE Antennas Wireless Propag. Lett.* **9**, 501 (2010).
- [24] W. Liu and Y. S. Kivshar, Generalized kerker effects in

- nanophotonics and meta-optics, *Opt. Express* **26**, 13085 (2018).
- [25] S. Person, M. Jain, Z. Lapin, J. J. Sáenz, G. Wicks, and L. Novotny, Demonstration of zero optical backscattering from single nanoparticles, *Nano Lett.* **13**, 1806 (2013).
- [26] I. M. Hancu, A. G. Curto, M. Castro-López, M. Kuttge, and N. F. van Hulst, Multipolar interference for directed light emission, *Nano Lett.* **14**, 166 (2013).
- [27] M. V. Rybin, D. S. Filonov, P. A. Belov, Y. S. Kivshar, and M. F. Limonov, Switching from visibility to invisibility via fano resonances: theory and experiment, *Sci. Rep.* **5**, 8774 (2015).
- [28] A. E. Miroshnichenko, A. B. Evlyukhin, Y. F. Yu, R. M. Bakker, A. Chipouline, A. I. Kuznetsov, B. Luk'anchuk, B. N. Chichkov, and Y. S. Kivshar, Nonradiating anapole modes in dielectric nanoparticles, *Nat. Commun.* **6**, 8069 (2015).
- [29] B. Luk'anchuk, R. Paniagua-Domínguez, A. I. Kuznetsov, A. E. Miroshnichenko, and Y. S. Kivshar, Suppression of scattering for small dielectric particles: anapole mode and invisibility, *Philos. Trans. R. Soc. A* **375**, 20160069 (2017).
- [30] A. Alu and N. Engheta, Multifrequency optical invisibility cloak with layered plasmonic shells, *Phys. Rev. Lett.* **100**, 113901 (2008).
- [31] A. Alù and N. Engheta, Cloaking and transparency for collections of particles with metamaterial and plasmonic covers, *Opt. Express* **15**, 7578 (2007).
- [32] M. V. Rybin, K. L. Koshelev, Z. F. Sadrieva, K. B. Samusev, A. A. Bogdanov, M. F. Limonov, and Y. S. Kivshar, High-q supercavity modes in subwavelength dielectric resonators, *Phys. Rev. Lett.* **119**, 243901 (2017).
- [33] K. Koshelev, G. Favraud, A. Bogdanov, Y. Kivshar, and A. Fratalocchi, Nonradiating photonics with resonant dielectric nanostructures, *Nanophotonics* **8**, 725 (2019).
- [34] S.-Y. Chiam, R. Singh, C. Rockstuhl, F. Lederer, W. Zhang, and A. A. Bettiol, Analogue of electromagnetically induced transparency in a terahertz metamaterial, *Phys. Rev. B* **80**, 153103 (2009).
- [35] R. Alae, C. Rockstuhl, and I. Fernandez-Corbaton, An electromagnetic multipole expansion beyond the long-wavelength approximation, *Opt. Commun.* **407**, 17 (2018).
- [36] P. Grahn, A. Shevchenko, and M. Kaivola, Electromagnetic multipole theory for optical nanomaterials, *New J. Phys.* **14**, 093033 (2012).
- [37] A. B. Evlyukhin, T. Fischer, C. Reinhardt, and B. N. Chichkov, Optical theorem and multipole scattering of light by arbitrarily shaped nanoparticles, *Phys. Rev. B* **94**, 1 (2016).
- [38] M. Kerker, D.-S. Wang, and C. Giles, Electromagnetic scattering by magnetic spheres, *JOSA* **73**, 765 (1983).
- [39] K. Frizyuk, Second-harmonic generation in dielectric nanoparticles with different symmetries, *JOSA B* **36**, F32 (2019).
- [40] K. Frizyuk, I. Volkovskaya, D. Smirnova, A. Poddubny, and M. Petrov, Second-harmonic generation in Mie-resonant dielectric nanoparticles made of noncentrosymmetric materials, *Phys. Rev. B* **99**, 075425 (2019).
- [41] J. Mäkitalo, M. Kauranen, and S. Suuriniemi, Modes and resonances of plasmonic scatterers, *Phys. Rev. B* **89**, 165429 (2014).
- [42] R. N. S. Suryadharma, M. Fruhnert, I. Fernandez-Corbaton, and C. Rockstuhl, Studying plasmonic resonance modes of hierarchical self-assembled meta-atoms based on their transfer matrix, *Phys. Rev. B* **96**, 045406 (2017).
- [43] P. Lalanne, W. Yan, K. Vynck, C. Sauvan, and J.-P. Hugonin, Light interaction with photonic and plasmonic resonances, *Laser Photonics Rev.* **12**, 1700113 (2018).
- [44] M. Doost, W. Langbein, and E. A. Muljarov, Resonant-state expansion applied to three-dimensional open optical systems, *Phys. Rev. A* **90**, 013834 (2014).
- [45] E. Muljarov, W. Langbein, and R. Zimmermann, Brillouin-wigner perturbation theory in open electromagnetic systems, *Europhys. Lett.* **92**, 50010 (2011).
- [46] S. Lobanov, W. Langbein, and E. Muljarov, Resonant-state expansion applied to three-dimensional open optical systems: Complete set of static modes, *Phys. Rev. A* **100**, 063811 (2019).
- [47] E. L. Ivchenko and G. Pikus, *Superlattices and Other Heterostructures: Symmetry and Optical Phenomena*, Vol. 110 (Springer Science & Business Media, 2012).
- [48] A. Gelessus, <http://symmetry.jacobs-university.de>.
- [49] M. Tinkham, *Group Theory and Quantum Mechanics* (McGraw-Hill, New York, 1964).
- [50] Z. Xiong, Q. Yang, W. Chen, Z. Wang, J. Xu, W. Liu, and Y. Chen, On the constraints of electromagnetic multipoles for symmetric scatterers: eigenmode analysis, *Opt. Express* **28**, 3073 (2020).
- [51] L. Brillouin, Les problèmes de perturbations et les champs self-consistents, (1932).
- [52] L. Landau and E. Lifshitz, *Quantum Mechanics* (Pergamon, New York, 1977).
- [53] K. Ohtaka and Y. Tanabe, Photonic bands using vector spherical waves. iii. group-theoretical treatment, *J. Phys. Soc. Jpn.* **65**, 2670 (1996).
- [54] G. Goss, *Website of group symmetry* (2000).
- [55] A. Gelessus, W. Thiel, and W. Weber, Multipoles and symmetry, *J. Chem. Educ.* **72**, 505 (1995).
- [56] M. Gorodetsky and V. Ilchenko, High-q optical whispering-gallery microresonators: precession approach for spherical mode analysis and emission patterns with prism couplers, *Opt. Commun.* **113**, 133 (1994).
- [57] S. Hayami, M. Yatsushiro, Y. Yanagi, and H. Kusunose, Classification of atomic-scale multipoles under crystallographic point groups and application to linear response tensors, *Phys. Rev. B* **98**, 165110 (2018).
- [58] A. N. Serdikov, I. V. Semchenko, and S. Tertyakov, *Electromagnetics of Bi-anisotropic Materials: Theory and Application*, Vol. 11 (Gordon and Breach, Amsterdam, 2001).
- [59] A. A. Bogdanov, K. L. Koshelev, P. V. Kapitanova, M. V. Rybin, S. A. Gladyshev, Z. F. Sadrieva, K. B. Samusev, Y. S. Kivshar, and M. F. Limonov, Bound states in the continuum and fano resonances in the strong mode coupling regime, *Adv. Photon.* **1**, 016001 (2019).
- [60] W. Chen, Y. Chen, and W. Liu, Multipolar conversion induced subwavelength high-q kerker supermodes with unidirectional radiations, *Laser Photon. Rev.* **13**, 1900067 (2019).
- [61] K. Koshelev, S. Kruk, E. Melik-Gaykazyan, J.-H. Choi, A. Bogdanov, H.-G. Park, and Y. Kivshar, Subwavelength dielectric resonators for nonlinear nanophotonics, *Science* **367**, 288 (2020).
- [62] H. Friedrich and D. Wintgen, Interfering resonances and bound states in the continuum, *Phys. Rev. A* **32**, 3231 (1985).

- [63] H. Cao and J. Wiersig, Dielectric microcavities: Model systems for wave chaos and non-hermitian physics, *Rev. Mod. Phys.* **87**, 61 (2015).
- [64] D. A. Varshalovich, A. N. Moskalev, and V. K. Khersonsky, *Quantum Theory of Angular Momentum: Irreducible Tensors, Spherical Harmonics, Vector Coupling Coefficients, 3nj Symbols* (World Scientific, Singapore, 1988).
- [65] E. P. Wigner and J. J. Griffin, *Group Theory and Its Application to The Quantum Mechanics of Atomic Spectra* (Academic Press inc, London, 1959).
- [66] G. Aubert, An alternative to Wigner d-matrices for rotating real spherical harmonics, *AIP Advances* **3**, 062121 (2013).
- [67] H. Zhang and Y. Han, Addition theorem for the spherical vector wave functions and its application to the beam shape coefficients, *J. Opt. Soc. Am. B* **25**, 255 (2008).
- [68] S. Stein, Addition theorems for spherical wave functions, *Q. Appl. Math.* **19**, 15 (1961).